THE ASTROPHYSICAL JOURNAL, 628:L97–L100, 2005 August 1

CAUSTIC AND WEAK-LENSING ESTIMATORS OF GALAXY CLUSTER MASSES

ANTONALDO DIAFERIO,[1] MARGARET J. GELLER,[2] AND KENNETH J. RINES[3]

Received 2005 April 28; accepted 2005 June 21; published 2005 July 19

ABSTRACT

There are only two methods for estimating the mass distribution in the outer regions of galaxy clusters, where virial equilibrium does not hold: weak gravitational lensing and identification of caustics in redshift space. For the first time, we apply both methods to three clusters: Abell 2390, MS 1358.4+6245, and Cl 0024+1654. The two measures are in remarkably good agreement out to $\sim 2\ h^{-1}$ Mpc from the cluster centers. This result demonstrates that the caustic technique is a valuable complement to weak lensing. With a few tens of redshifts per square comoving megaparsec within the cluster, the caustic method is applicable for any $z \lesssim 0.5$.

Subject headings: cosmology: miscellaneous — cosmology: observations — galaxies: clusters: individual (Abell 2390, Cl 0024+1654, MS 1358.4+6245) — gravitational lensing

1. INTRODUCTION

The relative distributions of mass and light in the universe have remained a profound and central mystery in cosmology for more than 70 years. Since Zwicky's pioneering use of the virial theorem to discover dark matter in the Coma Cluster (Zwicky 1933), the range and sophistication of methods for estimating cluster masses and mass profiles have increased to include a host of dynamical measures, X-ray estimates, and strong and weak gravitational lensing determinations.

Different mass estimators applied to rich clusters of galaxies constrain the mass distribution on different scales. Strong lensing generally provides constraints on very small scales ($\lesssim 0.1\ h^{-1}$ Mpc). Virial mass estimates, including Jeans analysis, assume dynamical equilibrium and apply only within the virial radius. Mass estimates based on X-ray observations assume hydrostatic equilibrium and rarely extend beyond one-half of the virial radius (Majerowicz et al. 2002; Pratt & Arnaud 2002).

At larger clustercentric radii where equilibrium assumptions break down, there exist only two techniques for mass estimation: weak lensing (Kaiser et al. 1995) and the redshift-space caustic technique (Diaferio & Geller 1997; Diaferio 1999, hereafter D99). Both techniques enable determination of the mass distribution from the cluster center to distances larger than the virial radius.

The caustic technique has been applied to many local clusters (Rines et al. 2003 and references therein). At small clustercentric radii, caustic estimates agree well with the traditional virial analyses in the optical and X-ray bands. At larger radii the caustic technique is still valid, but its mass estimates were tested against *N*-body simulations only (D99).

Here we discuss the first comparison of mass estimates from the caustic technique and weak lensing. Only recently have sufficient lensing and spectroscopic data become available to make this comparison. Both techniques have known systematic uncertainties: these comparisons test the importance of these systematics. In this Letter, we examine mass-profile measurements for three intermediate-redshift clusters: Abell 2390, MS 1358.4+6245, and Cl 0024+1654.

[1] Dipartimento di Fisica Generale "Amedeo Avogadro," Università degli Studi di Torino, via P. Giuria 1, I-10125 Torino, Italy; diaferio@ph.unito.it.

[2] Smithsonian Astrophysical Observatory, 60 Garden Street, Cambridge, MA 02138; mjg@cfa.harvard.edu.

[3] Yale Center for Astronomy and Astrophysics, Yale University, P.O. Box 208121, New Haven, CT 06520; krines@astro.yale.edu.

2. THE CAUSTIC TECHNIQUE

Cluster galaxies plotted in a redshift-space diagram (line-of-sight velocity v vs. projected distance R from the cluster center) distribute in a characteristic trumpet shape. The boundaries of this trumpet are called caustics (Kaiser 1987; Regős & Geller 1989). By assuming spherical symmetry and hierarchical clustering for the formation of the large-scale structure, the caustic mass estimator relates the caustic amplitude, the trumpet width in v at each radius R, $\mathcal{A}(R)$, to the escape velocity from the gravitational potential well generated by the cluster (Diaferio & Geller 1997).

The procedure developed in D99 provides an automatic method for locating the caustics and determining their amplitude. First, the procedure arranges all the galaxies in the field in a binary tree and finds the cluster members. The cluster members determine the center of the cluster, its one-dimensional velocity dispersion $\langle v^2 \rangle^{1/2}$, and its radius $\langle R \rangle$, the mean projected distance of the members from the cluster center. Table 1 lists these quantities for the three clusters.

The procedure next determines the threshold κ that enters the caustic equation, $f_q(R, v) = \kappa$. Here $f_q(R, v)$ is the galaxy density distribution in the redshift diagram, smoothed with an adaptive kernel. The parameter q sets the scaling between the quantities R and v. We choose the parameter κ by minimizing the quantity $S(\kappa, \langle R \rangle) = |\langle v^2_{\rm esc} \rangle_{\kappa,\langle R \rangle} - 4\langle v^2 \rangle|^2$, where $\langle v^2_{\rm esc} \rangle_{\kappa,\langle R \rangle} = \int_0^{\langle R \rangle} \mathcal{A}^2(R)\varphi(R)dR / \int_0^{\langle R \rangle} \varphi(R)dR$ is the mean caustic amplitude within $\langle R \rangle$ and $\varphi(R) = \int f_q(R, v)dv$.

D99 shows that the three-dimensional cumulative mass profile can now be estimated as

$$GM(<r) = \frac{1}{2} \int_0^r \mathcal{A}^2(R)dR. \qquad (1)$$

The error bars on individual data points are proportional to the inverse of the galaxy number density within the caustics (D99). This recipe quantifies the uncertainty in the mass estimate, which mostly results from deviations from spherical symmetry. The recipe was calibrated on *N*-body simulations (Kauffmann et al. 1999) that generally showed less cleanly defined caustics than in the real universe. Therefore, we suspect that these un-

TABLE 1
CLUSTER PARAMETERS

Cluster (1)	FOV ($\alpha \times \delta$) (2)	$N_{\rm field} \in [z_1, z_2]$ (3)	N (4)	α (J2000) (5)	δ (J2000) (6)	z (7)	$\langle v^2 \rangle^{1/2}$ (8)	$\langle R \rangle$ (9)	r_s (10)	c (11)	r_{200} (12)
A2390	43.8 × 7.4	351 ∈ [0.1, 0.4]	210	21 53 35.53	17 42 03.16	0.2284	1154	0.85	0.14 ± 0.17	11 ± 12	1.5 ± 2.4
MS 1358	20.9 × 21.4	360 ∈ [0.1, 0.5]	282	13 59 49.65	62 30 55.87	0.3289	996	0.76	0.14 ± 0.09	7.7 ± 4.3	1.1 ± 0.9
Cl 0024	20.0 × 24.3	399 ∈ [0.3, 0.5]	251	00 26 35.90	17 09 41.10	0.3941	937	0.74	0.12 ± 0.11	8.6 ± 7.7	1.0 ± 1.3

NOTE.—Col. (2), field of view (FOV), in arcminutes; col. (3), number of galaxies in the FOV within the redshift range $[z_1, z_2]$; col. (4), number of members; cols. (5)–(7), cluster center coordinates; col. (8), cluster velocity dispersion; col. (9), cluster size; cols. (10)–(12), NFW fit parameters. Velocities are in kilometers per second, lengths in h^{-1} Mpc. Units of right ascension are hours, minutes, and seconds, and units of declination are degrees, arcminutes, and arcseconds.

certainties are smaller for real clusters than in the simulations. The small scatter ($\lesssim$30%) around the equivalence relation between X-ray and caustic masses (Rines et al. 2003) suggests that the simulations indeed overestimate the errors in the caustic technique at small radii. If 30% represents a rough estimate of the correct caustic mass uncertainty at all radii, the D99 recipe typically overestimates this uncertainty by a factor of 2. Nevertheless, because it is the only available prescription for evaluating the error, we use the conservative D99 prescription. Comparison of gravitational lensing and caustic measurements for large samples of clusters in the redshift range 0.2–0.8 will test the accuracy of this recipe.

3. MASS COMPARISON

Mass-profile estimates of high-redshift clusters depend on the assumed cosmological parameters: physical distances and X-ray and weak-lensing cumulative mass profiles scale as the angular diameter distance D_A. Moreover, if one derives a best-fitting NFW (Navarro et al. 1997) density profile $\rho(r, z) = \delta_c \rho_{\rm crit}(z)(r/r_s)^{-1}(1 + r/r_s)^{-2}$, with $\rho_{\rm crit}(z) = 3H^2(z)/8\pi G$ the critical density of the universe, $H^2(z) = H_0^2[\Omega_0(1 + z)^3 + (1 - \Omega_0 - \Omega_\Lambda)(1 + z)^2 + \Omega_\Lambda]$, $\delta_c = c^3(200/3)[\ln(1 + c) - c/(1 + c)]^{-1}$, and $c = r_{200}/r_s$ the concentration parameter, c also depends (nonlinearly) on D_A, because $\delta_c \rho_{\rm crit}(z)$ scales as D_A^{-2}. Below, all quantities assume $\Omega_0 = 0.3$, $\Omega_\Lambda = 0.7$, and $H_0 = 100\ h$ km s^{-1} Mpc^{-1}.

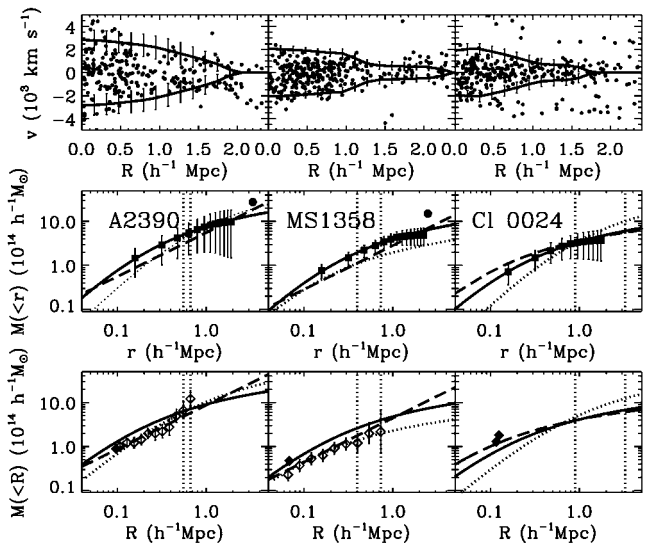

FIG. 1.—Redshift diagrams and mass profiles for A2390 (*left*), MS 1358 (*middle*), and Cl 0024 (*right*). *Top*: Redshift diagrams with the galaxies (*dots*) and caustic locations (*solid lines*). Line-of-sight velocities v are in the cluster rest frame. *Middle*: Three-dimensional cumulative mass profiles. The squares show the caustic mass estimates, the solid lines are the best-fitting NFW profiles to the data points within 1 h^{-1} Mpc, the dotted lines are the best-fitting NFW profiles to the X-ray measures (*left to right*: Allen et al. 2001; Arabadjis et al. 2002; Ota et al. 2004), and the dashed lines are the best-fitting isothermal (A2390, Squires et al. 1996; MS 1358, Hoekstra et al. 1998) or NFW (Cl 0024, Kneib et al. 2003) models to the gravitational lensing measures. The left and right vertical dotted lines show the radius of the X-ray and gravitational lensing fields of view, respectively. The two filled circles show the virial estimates by Carlberg et al. (1996) of A2390 and MS 1358. *Bottom*: Projected cumulative mass profiles; lines are as in the middle panels. The open diamonds show the weak-lensing measures: A2390, Squires et al. (1996); MS 1358, lower limit by Hoekstra et al. (1998) to the mass profile. Filled diamonds show the strong-lensing measures: A2390, Pierre et al. (1996); MS 1358, Allen (1998) from the measurement by Franx et al. (1997); Cl 0024, upper symbol, Tyson et al. (1998), lower symbol, Broadhurst et al. (2000). Error bars in all panels are 1 σ; error bars on points where they seem to be missing are smaller than the symbol size.

Figure 1 shows the redshift diagrams of the three clusters with the caustic location (*top*) and the mass profiles estimated with the caustic technique, gravitational lensing, and X-ray data (*middle and bottom*). Gravitational lensing measures all the mass projected onto the sky along the line of sight. Therefore, we distinguish between three-dimensional (*middle*) and projected (*bottom*) cumulative mass profiles. Radial distances are three-dimensional (r) or projected onto the sky (R).

The solid lines in the middle and bottom rows of Figure 1 show the best-fitting NFW profile with parameters listed in Table 1. To compute these fits, we only used the data points within $r_{\rm lim} = 1\ h^{-1}$ Mpc, a conservative radius beyond which the NFW mass profile might not be a good description of the actual profile. For all clusters, the data points beyond 1 h^{-1} Mpc do indeed agree with the NFW model, indicating that the correct choice of $r_{\rm lim}$ is irrelevant. In any case, the fit parameters and their errors are only indicative, because the individual data points are correlated. Moreover, the NFW fit parameters are correlated even with independent data points. Keeping one of the two parameters, c or r_s, fixed in our fits reduces their relative errors to ~10%.

For each cluster, we also show the best fits determined from the weak-lensing (*dashed lines*) and X-ray (*dotted lines*) measurements. We now comment on each cluster separately.

A2390.—This is a rich cluster at $z = 0.228$ with optical (Le Borgne et al. 1991; Yee et al. 1996), X-ray (Böhringer et al. 1998; Allen et al. 2001), and both weak (Squires et al. 1996) and strong (Pelló et al. 1991; Pierre et al. 1996) gravitational lensing observations. Squires et al. (1996) compared the weak-lensing data within ~260″ with a singular isothermal model with velocity dispersion $\sigma = 1093$ km s^{-1} taken from Carlberg et al. (1996). The isothermal model underpredicts the amount of mass actually measured in the range 0.46–0.67 h^{-1} Mpc (Fig. 1, *bottom left*); however, this model is in good agreement with the best-fitting NFW mass profile derived by Allen et al. (2001) from *Chandra* observations. They find $r_s = 0.44^{+0.76}_{-0.22}$ h^{-1} Mpc, $c = 3.6^{+2.0}_{-1.6}$, and $r_{200} = 1.6^{+2.9}_{-1.1}\ h^{-1}$ Mpc.

By using the galaxy redshift survey by Yee et al. (1996) and assuming dynamical equilibrium, Carlberg et al. (1996) estimate a mass $M(<3.3\ h^{-1}\ {\rm Mpc}) = (2.7 \pm 0.4) \times 10^{15}\ h^{-1}\ M_\odot$. The caustic mass $(1.4 \pm 1.2) \times 10^{15}\ h^{-1}\ M_\odot$ and the mass $1.8 \times 10^{15}\ h^{-1}\ M_\odot$ extrapolated from the weak-lensing isothermal

model are 48% and 33% smaller than this virial mass, but within its $3\,\sigma$ uncertainty.

At smaller radii, A2390 sports spectacular arcs and arclets (Pelló et al. 1991), some of which have measured redshifts (Bézecourt & Soucail 1997; Frye & Broadhurst 1998; Pelló et al. 1999). Pierre et al. (1996) used the brightest strongly lensed arc and its surrounding shear to derive the projected total enclosed mass $M(<97\ h^{-1}\ \mathrm{kpc}) = (8.0 \pm 1.0) \times 10^{13}\ h^{-1}\ M_{\odot}$[4] (Fig. 1, *filled diamond*), in agreement with the mass $(1.2 \pm 0.7) \times 10^{14}\ h^{-1}\ M_{\odot}$ implied by the projection of the NFW fit to the caustic mass; the strong-lensing mass also agrees with the mass $8.5 \times 10^{13}\ h^{-1}\ M_{\odot}$ implied by the weak-lensing isothermal model and is just above the 68% confidence bound derived with the X-ray analysis (Fig. 8 of Allen et al. 2001).

Pierre et al. (1996) derived the strong-lensing mass by assuming that the arc is a single lensed galaxy at $z = 0.913$. Frye & Broadhurst (1998) later showed that the fainter part of this arc actually is a second lensed galaxy at $z = 1.033$. The redshifts of the arcs and arclets, which are available now but were not at the time of Pierre et al.'s analysis, urge a reformulation of the lensing model of the core of A2390. However, we expect that a newly derived mass will not substantially differ from the mass of Pierre et al. (1996), because the mass estimated with the simplest lensing models, which provide the most inaccurate measures, probably are within 30% of the true value (Kochaneck et al. 2005).

MS 1358.4+6245.—This is a very rich cluster first discovered by Zwicky & Herzog (1968). We collect 381 redshifts in the cluster region from the surveys of Fabricant et al. (1991), Fisher et al. (1998), and Yee et al. (1998).

Hoekstra et al. (1998) used *Hubble Space Telescope* observations to construct a weak-lensing map of the cluster extending to a radius of $\sim 220'' = 0.73\ h^{-1}$ Mpc. They only derive a lower limit to the mass profile and find a best-fitting singular isothermal model with $\sigma = 780 \pm 50$ km s^{-1} (Fig. 1, *dashed lines*). More recently, Arabadjis et al. (2002) analyzed a *Chandra* observation of the cluster. They approximate the mass profile within $\sim 2' = 0.4\ h^{-1}$ Mpc with an NFW profile, with $r_s = 88^{+92}_{-47}\ h^{-1}$ kpc, $c = 9.3^{+3.8}_{-2.5}$, and $r_{200} = 0.81^{+0.92}_{-0.49}\ h^{-1}$ Mpc.

Carlberg et al. (1996) assumed virial equilibrium to estimate $M(<2.5\ h^{-1}\ \mathrm{Mpc}) = (1.5 \pm 0.2) \times 10^{15}\ h^{-1}\ M_{\odot}$ from their galaxy redshift survey. This mass is more than $3\,\sigma$ above the weak-lensing isothermal extrapolation $7.0 \times 10^{14}\ h^{-1}\ M_{\odot}$, which agrees with the caustic estimate $(6.5 \pm 2.8) \times 10^{14}\ h^{-1}\ M_{\odot}$. The extrapolation of the X-ray fit yields $3.0 \times 10^{14}\ h^{-1}\ M_{\odot}$, a factor of 2 smaller than the caustic mass and a factor of 5 below the virial mass. Probably, the assumption of virial equilibrium at this large distance is unrealistic and the extrapolation of the X-ray profile, limited to radii of less than $0.4\ h^{-1}$ Mpc, is unreliable.

In the very central region, Allen (1998) used the strong-lensing observations by Franx et al. (1997) to derive a projected mass $M(<69\ h^{-1}\ \mathrm{kpc}) = 4.4 \times 10^{13}\ h^{-1}\ M_{\odot}$ with a 20% uncertainty. The projected NFW profile derived from the caustics yields a perfectly consistent mass $(4.2 \pm 1.3) \times 10^{13}\ h^{-1}\ M_{\odot}$. The projected profiles derived by Hoekstra et al. (1998) and Arabadjis et al. (2002) imply the somewhat lower masses 3.0×10^{13} and $2.9 \times 10^{13}\ h^{-1}\ M_{\odot}$, respectively.

[4] In this Letter, we rescale each strong-lensing mass found in the literature by the effective lensing distance $D_l D_{ls}/D_s$ appropriate to a universe with $\Omega_0 = 0.3$ and $\Omega_\Lambda = 0.7$; D_l, D_s, and D_{ls} are the angular distances to the cluster, to the source of the lensed image, and between the cluster and the source, respectively.

The X-ray and weak-lensing mass models agree within $\sim 0.8\ h^{-1}$ Mpc but underestimate the strong-lensing mass derived by Allen (1998). The fact that the weak-lensing mass provides only a lower limit to the mass profile and the caustic mass is in excellent agreement with the strong-lensing measurement suggests that the caustic mass provides the correct mass profile of MS 1358 out to $\sim 2\ h^{-1}$ Mpc.

Cl 0024+1654.—Significant tension exists between lensing (Bonnet et al. 1994; Tyson et al. 1998) and X-ray (Soucail et al. 2000; Ota et al. 2004) mass estimates of this cluster. Kneib et al. (2003) combine their weak-lensing measurements from wide-field imaging with the strong-lensing measurement by Broadhurst et al. (2000) to derive the best-fitting NFW profile, with $r_s = 54 \pm 2\ h^{-1}$ kpc, $c = 18.7^{+7.7}_{-4.3}$, and $r_{200} = 1.01^{+0.41}_{-0.23}\ h^{-1}$ Mpc. According to their Figure 12, the uncertainty in their mass estimate is always $\lesssim 10\%$. Our Figure 1 also shows the NFW profile that fits recent *Chandra* data (Ota et al. 2004). These authors derive the NFW profile from a β-model fit. According to its parameters, we find $r_s = 0.56 \pm 0.02\ h^{-1}$ Mpc, $c = 1.8 \pm 0.3$, and $r_{200} = 1.02 \pm 0.18\ h^{-1}$ Mpc. Our caustic estimate (based mostly on the spectroscopy of Czoske et al. 2001) lies between the lensing and the X-ray fits at $r < 0.2\ h^{-1}$ Mpc, but it is in excellent agreement with the lensing estimate outside $\sim 0.5\ h^{-1}$ Mpc.

In the cluster central region there are two strong-lensing measurements, which yield comparable masses. However, the very small errors claimed make them inconsistent with each other: $M(<0.114\ h^{-1}\ \mathrm{Mpc}) = (1.30 \pm 0.04) \times 10^{14}\ h^{-1}\ M_{\odot}$ (Broadhurst et al. 2000) and $M(<0.119\ h^{-1}\ \mathrm{Mpc}) = (1.563 \pm 0.002) \times 10^{14}\ h^{-1}\ M_{\odot}$ (Tyson et al. 1998). We scaled the mass reported by Tyson et al. (1998) by assuming $z = 1.675$ for the arc, as measured by Broadhurst et al. (2000). By construction, the NFW profile of Kneib et al. (2003) agrees with the former [it yields $M(<0.114\ h^{-1}\ \mathrm{Mpc}) = 1.13 \times 10^{14}\ h^{-1}\ M_{\odot}$] and therefore disagrees with the latter [it yields $M(<0.119\ h^{-1}\ \mathrm{Mpc}) = 1.17 \times 10^{14}\ h^{-1}\ M_{\odot}$]. The caustic profile gives smaller, but consistent, masses in both cases: $(7.9 \pm 3.8) \times 10^{13}$ and $(8.5 \pm 4.0) \times 10^{13}\ h^{-1}\ M_{\odot}$, respectively. The NFW fit to the X-ray data yields even smaller masses: 3.8×10^{13} and $4.2 \times 10^{13}\ h^{-1}\ M_{\odot}$ with a $\sim 30\%$ typical error. Czoske et al. (2002) suggest that the peculiar-redshift distribution of the galaxies within $\sim 3.5\ h^{-1}$ Mpc of the cluster center can be explained by a high-speed collision along the line of sight between Cl 0024 and a less massive cluster. This model implies that the X-ray mass estimate based on dynamical equilibrium is unreliable. Because the caustic and lensing mass estimators are both independent of the dynamical state of the cluster, it is reasonable that they agree with each other but disagree with the X-ray mass.

4. CONCLUSION

For the first time, we compare the only two cluster mass estimators that do not rely on the dynamical equilibrium of the system: weak gravitational lensing and caustics in redshift space. We estimate the caustic mass of A2390, MS 1358, and Cl 0024 within $\sim 2\ h^{-1}$ Mpc of the cluster centers. The caustic mass profiles are in very good agreement with the lensing profiles. We confirm that the discrepancy between lensing and X-ray mass in Cl 0024 is probably a consequence of the unrelaxed state of the cluster, which invalidates the X-ray analysis.

Weak lensing requires accurate photometric wide-field surveys in excellent seeing; moreover, the cluster sample is somewhat limited to clusters at distances where the lensing signal is sufficiently strong. Weak lensing measures all the mass pro-

jected along the line of sight, resulting in a minimum 20% uncertainty in the cluster mass estimates (de Putter & White 2005). The caustic technique, which requires dense wide-field redshift surveys, provides a complementary measurement of the three-dimensional mass profile of individual clusters at moderate redshift; it also yields robust mass profiles for clusters in the local universe.

Future comparison of these techniques for large samples of clusters, covering a range of redshifts, will constrain systematic uncertainties in the methods and may provide insight into the change in the relative amounts of mass in the infall regions and cluster cores as a function of look-back time.

We thank the referee for noticing a few inaccuracies in the first version of this Letter. We have made use of NASA's Astrophysics Data System and the NASA/IPAC Extragalactic Database (NED), operated by the Jet Propulsion Laboratory, California Institute of Technology, under contract with NASA.

REFERENCES

Allen, S. W. 1998, MNRAS, 296, 392
Allen, S. W., Ettori, S., & Fabian, A. C. 2001, MNRAS, 324, 877
Arabadjis, J. S., Bautz, M. W., & Garmire, G. P. 2002, ApJ, 572, 66
Bézecourt, J., & Soucail, G. 1997, A&A, 317, 661
Böhringer, H., Tanaka, Y., Mushotzky, R. F., Ikebe, Y., & Hattori, M. 1998, A&A, 334, 789
Bonnet, H., Mellier, Y., & Fort, B. 1994, ApJ, 427, L83
Broadhurst, T., Huang, X., Frye, B., & Ellis, R. 2000, ApJ, 534, L15
Carlberg, R. G., Yee, H. K. C., Ellingson, E., Abraham, R., Gravel, P., Morris, S., & Pritchet, C. J. 1996, ApJ, 462, 32
Czoske, O., Kneib, J.-P., Soucail, G., Bridges, T. J., Mellier, Y., & Cuillandre, J.-C. 2001, A&A, 372, 391
Czoske, O., Moore, B., Kneib, J.-P., & Soucail, G. 2002, A&A, 386, 31
de Putter, R., & White, M. 2005, NewA, 10, 676
Diaferio, A. 1999, MNRAS, 309, 610 (D99)
Diaferio, A., & Geller, M. J. 1997, ApJ, 481, 633
Fabricant, D. G., McClintock, J. E., & Bautz, M. W. 1991, ApJ, 381, 33
Fisher, D., Fabricant, D., Franx, M., & van Dokkum, P. 1998, ApJ, 498, 195
Franx, M., Illingworth, G. D., Kelson, D. D., van Dokkum, P. G., & Tran, K.-V. 1997, ApJ, 486, L75
Frye, B., & Broadhurst, T. 1998, ApJ, 499, L115
Hoekstra, H., Franx, M., Kuijken, K., & Squires, G. 1998, ApJ, 504, 636
Kaiser, N. 1987, MNRAS, 227, 1
Kaiser, N., Squires, G., & Broadhurst, T. 1995, ApJ, 449, 460
Kauffmann, G., Colberg, J. M., Diaferio, A., & White, S. D. M. 1999, MNRAS, 303, 188
Kneib, J.-P., et al. 2003, ApJ, 598, 804
Kochaneck, C. S., Schneider, P., & Wambsganss, J. 2005, Gravitational Lensing: Strong, Weak, and Micro (Berlin: Springer), in press
Le Borgne, J.-F., Mathez, G., Mellier, Y., Pelló, R., Sanahuja, B., & Soucail, G. 1991, A&AS, 88, 133
Majerowicz, S., Neumann, D. M., & Reiprich, T. H. 2002, A&A, 394, 77
Navarro, J. F., Frenk, C. S., & White, S. D. M. 1997, ApJ, 490, 493
Ota, N., Pointecouteau, E., Hattori, M., & Mitsuda, K. 2004, ApJ, 601, 120
Pelló, R., Le Borgne, J.-F., Soucail, G., Mellier, Y., & Sanahuja, B. 1991, ApJ, 366, 405
Pelló, R., et al. 1999, A&A, 346, 359
Pierre, M., Le Borgne, J.-F., Soucail, G., & Kneib, J.-P. 1996, A&A, 311, 413
Pratt, G. W., & Arnaud, M. 2002, A&A, 394, 375
Regős, E., & Geller, M. J. 1989, AJ, 98, 755
Rines, K., Geller, M. J., Kurtz, M. J., & Diaferio, A. 2003, AJ, 126, 2152
Soucail, G., Ota, N., Böhringer, H., Czoske, O., Hattori, M., & Mellier, Y. 2000, A&A, 355, 433
Squires, G., Kaiser, N., Fahlman, G., Babul, A., & Woods, D. 1996, ApJ, 469, 73
Tyson, J. A., Kochanski, G. P., & dell'Antonio, I. P. 1998, ApJ, 498, L107
Yee, H. K. C., Ellingson, E., Abraham, R. G., Gravel, P., Carlberg, R. G., Smecker-Hane, T. A., Schade, D., & Rigler, M. 1996, ApJS, 102, 289
Yee, H. K. C., Ellingson, E., Morris, S. L., Abraham, R. G., & Carlberg, R. G. 1998, ApJS, 116, 211
Zwicky, F. 1933, Helvetica Phys. Acta, 6, 110
Zwicky, F., & Herzog, E. 1968, Catalogue of Galaxies and of Clusters of Galaxies, Vol. 4 (Pasadena: Caltech)